AN IMPROVED ENDMEMBER EXTRACTION ALGORITHM BY INVERSING LINEAR MIXING MODEL

LI Shanshan, TIAN Qingjiu

International Institute for Earth System Science, Nanjing University, Nanjing, 210093, China –lisslee@163.com

WG VII/3

KEY WORDS: Hyperspectral Remote Sensing, Spectral Indices, Image Understanding, Simulation, Extrapolation

ABSTRACT:

In hyperspectral imagery there are some cases when no pure pixels present due to the limitation of the sensors' space resolution and the complexity of the ground components, and then the endmembers extracted by traditional algorithms are usually mixing ones still. In order to solve this problem, this paper proposes an endmember extraction algorithm based on the re-analysis of preliminary endmembers extracted by volume calculating concept under the linear mixing model. After extracting the pixels which are most approximated to the pure pixels from the image, using the convex polyhedron's geometric characters to search out the boundary pixels which are around the preliminary endmembers and on the edge of the convex polyhedron formed by the pure pixels. Calculating the abundance fractions of every endmember in these pixels by the laws of sins, thus, with these coefficients the endmembers could be obtained using the inversion of linear mixing model. Hyperspectral scenes are simulated by the real spectra to investigate the performance of the algorithm. Preliminary results indicate the effectiveness of the algorithm. Applying the algorithm to a real Hyperion scene it also gets a better result.

1. INTRODUCTION

Hyperspectral remote sensing using imaging spectrometry technology automatically obtains the spectra information of ground targets. Pixels in the obtained images record nearly continuous spectra information with narrow bands, using these continuous spectra the ability of interpretation and classification of remotely sensed imagery have been greatly improved (Chen, Tong, 1998) .

Due to the limitation of the sensors' space resolution and the complexity and diversity of the ground components, most of the recorded pixels are mixed ones, thus the acquired spectra information is integrated response of few ground components spectra (Zhao, 2003). In order to improve the application precision of the pixel spectra, the problem of spectral mixing must be solved.

For the simpleness and easy disposing, linear spectral unmixing model (Keshava, Mustard, 2002) has been widely used in unmixing and classification of multi/hyperspectral datasets. The approach includes two steps (Bateson, Asner, Wessman, 2000): first, to find out pure ground components signatures, usually referred to as endmembers (Kruse, 1998); second, to model every pixel to the linear combination of endmembers. Generally, the spectrum of any given pixel in a hyperspectral image given with N bands is assumed to be a linear combination of endmember spectra:

$$R(x,y)=\sum_{i=1}^{e}E_i c_i+\varepsilon_i \qquad (1)$$

$$\sum_{i=1}^{e}c_i=1,\ 0\le c_i\le 1 \qquad (2)$$

Where: e is the number of endmember, $R(x,y)$ is a spectrum of pixel with coordinate(x,y), E_i is the endmember matrix, c_i is endmember abundance fraction matrix for corresponding pixel, and ε_i is Gaussian random error. For the ideal endmembers, pixel compositions are assumed to be percentages, the mixing proportion coefficients are constrained to be sum to one and nonnegative as shown in function (2). If the influence of noise ε_i is ignored, endmembers can be N dimensional vectors and every pixel is N−D vector mixed by endmembers. In N−D space, pixel vectors based on linear mixing model form a convex polyhedron in which endmembers are vertexes and all the other mixing pixels lie within it (Winter, 1999). A mixture model based on three or four endmembers in the N-dimensional hyperplane has the simple geometrical interpretation as the triangle or tetrahedron whose vertices are the endmembers. Cover fractions are determined by the comparative position of the modelled spectrum in the figure, which could be within the interior or on the boundary (Antonio, 2002) , as Fig.1 shows.

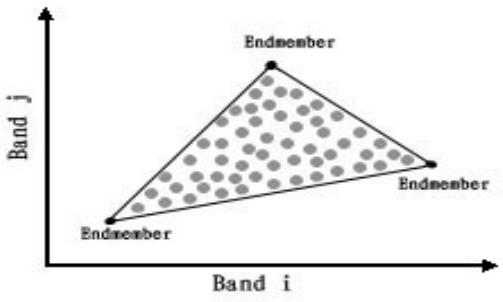

Figure 1. Scatter plot of 2-D spectral data illustrating the physical interpretation of a mixture model based on three endmembers.

Over the past decade, based on linear spectral unmixing model, scholars domestic and abroad proposed a number of well developed endmember extraction algorithms, such as: PPI (Theiler, 2000)、IEA (Staenz, 1998), ORASIS (Bowles, 1995), N-FINDR (Winter, 1999), AMEE (Antonio, 2002), CCA (Agustin, Chang, 1999), MEST (Bateson, 1993), etc. Some researchers studied the endmember extraction methods quantitatively and comparatively and got some important conclusions (Antonio, 2004). However, most existing endmember extraction algorithms are based on the assumption that endmembers exit and present in the images in the form of pure or unmixed pixels, through all kinds of algorithms the pure ones can be extracted from the image and be used as endmembers.

Oriented to solving the problem that the mixing spectra are ubiquitous and there may be case that no pure pixel exits in the imagery, this article proposes a new endmember extraction algorithm. Based on linear mixing model, the geometry of convex sets in N spectral dimensions illustrates that the N-volume formed of the pure pixels is larger than any other volume formed from any other combination of pixels (Winter, 1999). First the volume of convex polyhedron is calculated to extract the purest pixels which formed the possible largest volume, then search for the boundary pixels which are around the extracted pixels, using geometric relationship to calculate the fractional abundance of extracted endmembers in boundary pixels, finally using linear inversion the pure endmembers are obtained. Simulated hyperspectral images are synthesized to validate the effectiveness of this algorithm, and the algorithm has also been successfully applied on real hyperspectral imagery, advantages and shortages are commented.

2. ENDMEMBER EXTRACTION ALGORITHM

If there are no completely unmixed pixels exit in hyperspectral image, the pixels extracted by applying traditional methods are only the ones least mixed and most closely approximates the pure ones. In N-D space, outside the volume formed by the extracted pixels there are still other mixed pixels exit and these outside ones are within the biggest N-volume formed by the pure ones, only for that the vertices of the biggest N-volume do not appear in the image. And those pure pixels which did not present in the image are the object of this proposed algorithm. Fig.2 illustrates this situation formed by the combination of three endmembers, the extracted endmembers by only calculating the biggest N-volume in the image can not precisely represent the pure pixels in real.

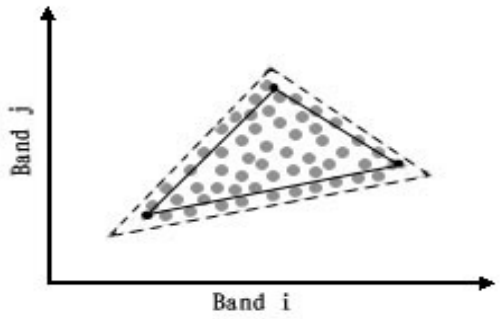

Figure 2. Sketch Map of the set of pixels with the largest possible volume, some mixed pixels are outside of this volume

This algorithm assumes that the endmembers themselves are not represented in the datasets. First using improved N-FINDR algorithm (Geng, 2006) to extract the preliminary pure pixels which form the largest possible volume in the image.

$$V_n = V(R_n - R_1, R_n - R_2, \Lambda, R_n - R_{n-1}) = \frac{1}{(n-1)!}\sqrt{|A_{n-1}^T A_{n-1}|} \qquad (3)$$

Where, $A_{n-1} = (R_n - R_1, R_n - R_2, \Lambda, R_n - R_{n-1})$, $R_i, (i = 1, \Lambda, n-1)$ is the pixel vector, (n-1) is the number of dimensions occupied by the data. This improved N-FINDR algorithm could extract pixels constructed the possible largest N-volume from the image without dimension reduction. Father analysis is needed to obtain the endmembers.

2.1 Three Components Mixing

When the ground components in the image are comparatively simple and mixed by three substances, the geometrical interpretation of the convex polyhedron constructed by all the pixels is a triangle. Calculate V_3 first, the extracted preliminary pure pixels are marked as S_1, S_2 and S_3. As shown in Fig.3, after extraction of S_1, S_2 and S_3, search around the neighbouring pixels in the hyper plane and find out the boundary pixels *A, B, C, D, E and F*. The selection of boundary points are required to stratified with next conditions.

(1) Boundary vectors are in the hyperplane formed by preliminary endmembers. In the image comprised of only three ground components, this condition are automatically matched. However, when the image contains more than three ground components, finding boundary points must meet this requirement. According to linear correlation of vectors in plane, $1 \times N$ dimensional row vectors S_1, S_2 and S_3 built up a $3 \times N$ dimensional matrix $[S_1, S_2, S_3]^T$ with the rank of three, with the spectral vectors of original image have been previously transposed. Calculate every rank of the $4 \times N$ matrix formed by the combination of each pixel vector R_i with S_1, S_2 and S_3, if the rank of this matrix is still three, the conclusion that R_i is linear correlated with S_1, S_2 and S_3 can be got which means R_i is in the hyperplane formed by S_1, S_2 and S_3.

(2) Boundary vectors are outside the convex polyhedron formed by the preliminary endmembers. If R_i is outside the triangle $S_1S_2S_3$, then the sum volume of three small triangles formed by R_i with every two of S_1, S_2 and S_3 respectively is greater than the volume of original largest triangle.

(3) Each boundary vector has the shortest distances to one of the preliminary endmembers respectively and the largest volume formed with other two preliminary endmembers.

Searching the pixels one by one, finally the six pixels meet the requirements above are obtained and can be approximately regarded as the boundary pixels on the edges of the triangle formed by preliminary endmembers.

The six boundary pixels on the edges of triangle in hyperplane are marked as *A, B, C, D, E and F*, linking the points one and another to form three line vectors *AB, CD, EF*. Let the pure pixel vectors signed as G_1, G_2, G_3, and the three points are the intersection of extension line of *AB, CD, and EF* in two opposite directions. Using geometric triangle relationship to calculate the vectors, based on functions:

$$\cos(x, y) = \frac{x \cdot y}{|x| \times |y|} \quad (4)$$

$$\frac{|x|}{\sin(X)} = \frac{|y|}{\sin(Y)} = \frac{|z|}{\sin(Z)} \quad (5)$$

Where, *x, y, z* are three edge vectors of a triangle, *X, Y, Z* are the corresponding angles. Through calculation $|G_1G_2|$, $|G_2G_3|$, $|G_3G_1|$ can be obtained. For the relative position of pixel vector within the convex polyhedron can be considered as the cover fractions of endmembers in pixel, the cover fractions of endmembers G_1, G_2, G_3 in *A, B, C, D, E and F* are calculated out, thus cover fraction matrix *C* is obtained. According to linear model, (1) is inversed as:

$$E = R / C \quad (6)$$

Given *C* and prior boundary point vectors *R* of three boundary pixels, endmember matrix *E* is the solution satisfies (6), thus with this inversion of linear mixing model the endmember vectors are obtained.

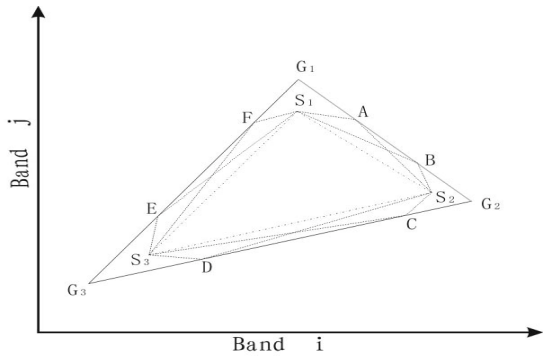

Figure 3. Structure scheme of the algorithm.

2.2 Four Ground Covers Mixing

This section considers the situation when the image contains four ground components or four components with greatest difference are required to be extracted. Four materials linear mixed a convex polyhedron in geometric interpretation turned out to be a tetrahedron in *N-D* space. First, V_4 is calculated, the four preliminary pure pixels are signed as S_1, S_2 , S_3 and S_4, as Fig.4 (a) shows. Then perpendicular is made from S_4 to the hyperplane formed by S_1, S_2 and S_3, intersection points signed as *M*. Next, search for boundary pixels *A, B, C, D, E and F* which are on the three arrises of the tetrahedron and around the preliminary endmembers. Spatial structure which the algorithm pursuant is shown in Fig.4 (b), the choice of boundary pixels meets following requests:

(1) Boundary pixels are located in the hyperplane formed by the combination of every two preliminary endmembers and the vertical point *M* respectively. This condition can be achieved with the method described above which need to search from three the vertical planes inside tetrahedron.

(2) Boundary pixels have the shortest distance with S_1, S_2, S_3 and S_4 respectively, and the combination of one of the boundary pixels, S_4 and one of S_1, S_2, S_3, correspondingly can form a triangle with largest volume.

(3) Boundary pixels in every two arrises are in a hyper plane, the rank of the matrix formed by each four vectors is three.

Search the pixels one by one, finally the six boundary pixels meet the requests are obtained. Within the triangles formed by the vertical line inside the tetrahedron and each arrises, four vertices of the tetrahedron G_1, G_2, G_3 and G_4 can be extracted out as pure pixels.

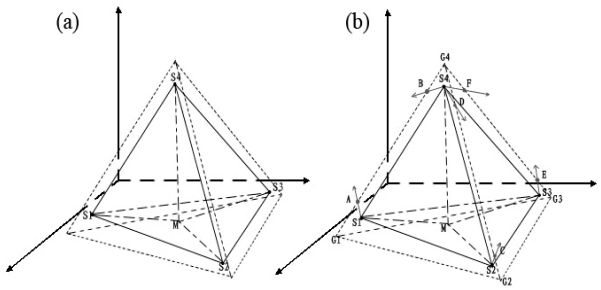

Figure 4. Four endmembers mixing. (a) The geometric interpretation of a tetrahedron. (b) Sketch map.

3. IMPLEMENTATION WITH SIMULATED DATA

Based on second-development platform of ENVI, the algorithm is implemented using IDL language, and simulated hyperspectral data are designed to evaluate the performance of the algorithm. Considering the mixing situation of three and four ground components respectively, two simulated images were generated.

3.1 Generation of Simulated Data

Three spectra were chosen from JUL spectral database (http://asterweb.jpl.nasa.gov/speclib/) in ENVI which presented soil, vegetation and manual target separately, and a water spectrum was chosen from spectral database commonly used. Resampling the four spectra, 50 bands with the wavelength covered from 508.220um to 1033.550um are saved, target spectra are shown in Fig.5. With different abundance fractions and the constraints of sum to one and nonnegative, two simulated image were designed under linear mixing model.

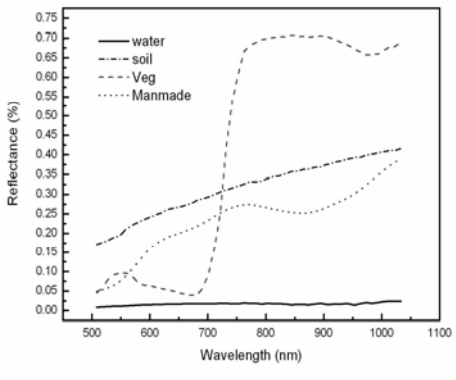

Figure 5. Original Reflectance Spectrum

First, soil, vegetation and manmade spectra were chosen to create a simulated hyperspectral data for implementation of three endmembers extraction. As Fig.6 (a) shows, the 60*60-pixel scene is formed by six regions of ten-pixel width. In every region, pixel spectra in each line are the same; in row direction,

the abundance of endmembers in pixels has a gradually changing process (mixing fraction shows in Table.1) and the abundance fractions of every ground components are no more than 0.95 to insure no pure pixels exit in the scene.

Region	Soil	Vegetation	Manmade
R1	(10/12)*(i/60)	0.5*[1-(10/12)*(i/60)]	0.5*[1-(10/12)*(i/60)]
R2	0.5*[1-(10/12)*(i/60)]	(10/12)*(i/60)	0.5*[1-(10/12)*(i/60)]
R3	0.5*[1-(10/12)*(i/60)]	0.5*[1-(10/12)*(i/60)]	(10/12)*(i/60)
R4	(2/3)*(1-i/120)	1-(2/3)*(1-i/120)	0
R5	0	(2/3)*(1-i/120)	1-(2/3)*(1-i/120)
R6	1-(2/3)*(1-i/120)	0	(2/3)*(1-i/120)
i=1,2,……60			

Table 1 Abundance assignment for regions in simulated scene

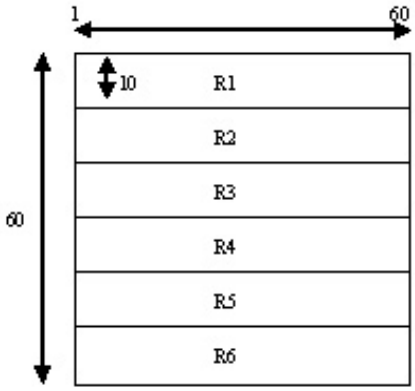

Figure 6. Sketch map of simulated scene with 3 components

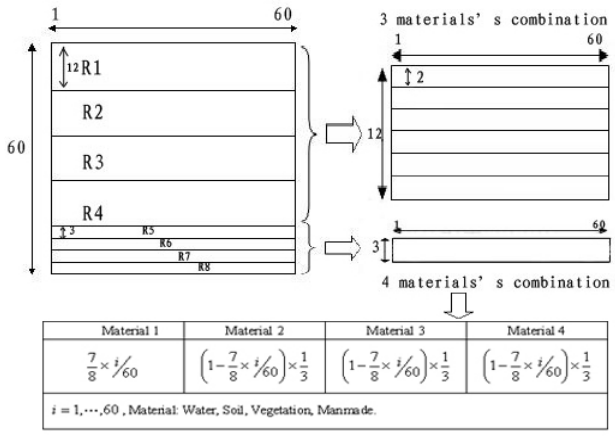

Figure 7. Sketch map of simulated scene with 4 components

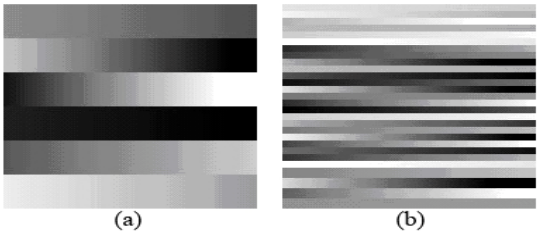

Figure 8. The band 23 images of two simulated scenes

Then all the four spectrum were chosen to create the second scene with a size of 60*60 pixels, and the data was parted into 8 regions in landscape orientation. The first four regions which all have the size of 2*60 pixels are formed with every three materials respectively. The abundance fraction of these regions is distributed as shown in fig.6 and tab.1. Due to the spectrum of water is distinguishedly different from the others, when there was water spectra in any of the four mixing regions, the max abundance fraction was changed to 11/12 but still no more than 0.95. The next four regions each with size of 3*60 pixels are all mixed by four materials and with one component has the largest abundance fraction in one region respectively. Every region's row direction still has a gradual changing of endmember abundance fractions. And with the abundance fraction of each components no more than 0.95, there is no pure pixel exit in the image. The images of band 23 of two simulated scenes are shown as Fig.8 (a), (b).

3.2 Evaluation with experimental results

Comparative analysis of endmember extracted with this proposed algorithm, original spectra and preliminary pure pixels extracted from the images using improved N-FINDR are illustrated in Fig.9 and Fig.10. Black solid lines present original spectra and black dashed lines are the preliminary endmembers, red solid lines are the spectra extracted with this researched algorithm. From the both graphs, red solid lines are well matched with the black solid lines. Although the black dashed lines are approximated to the black real ones, difference still exits, and this is caused by no pure pixels present in the data, the pixels extracted by traditional methods are most approximated to the original pure spectra, but still mixing ones. This researched algorithm based on the extracted possible purest pixels, search the boundary pixels and through using inversion of linear mixing model could successfully extracted the pure spectra which don't exit in the image.

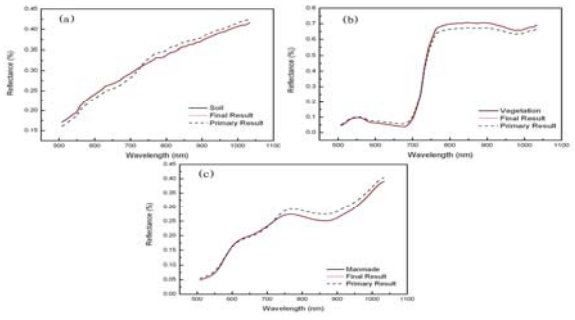

Figure 9. Comparison of three extracted endmembers with original spectra.(a) Soil, (b) Vegetation, (c) Manmade

Spectral similarity measurement between extracted spectra and original spectra are calculated using SCM, SAM and ED (Van

der Meer, 2006)\. As Tab.2 (a) illustrates the SCM values between the original spectra and this algorithm extracted ones are more close to 1 than the values between original spectra and the preliminary pure ones, and the new endmembers present higher spectral similarity to ground truth. The SAM and ED values of this algorithm also show the advantages correspondingly. Similarity analysis of four endmembers combination shows the same results as shown in Tab.2 (b).
The experiment results proved that, when the pixels in the image are all mixed and the image is combined by three or four components, the proposed algorithm can successfully extract the spectral vectors highly approximated to the ground truth.

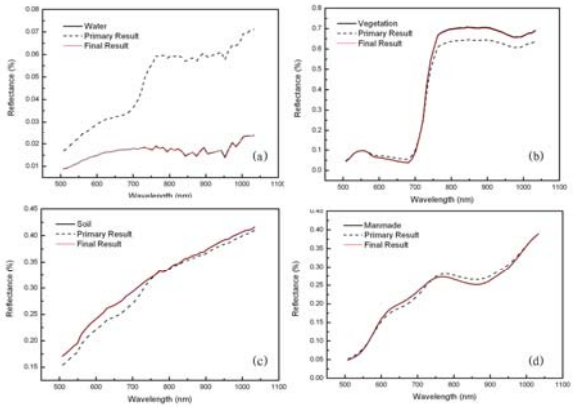

Figure 10. Comparison of four extracted endmembers with original spectra. (a) Water, (b) Vegetation, (c) Soil, (d) Manmade

(a) Three endmembers combination

Endmember		SCM	SAM	ED
C1	O/P	0. 99738815	0. 030642001	0. 043332638
	O/F	0. 99999998	0. 000039943	0. 000056489
C2	O/P	0. 99991274	0. 020130492	0. 028468334
	O/F	1. 0000000	0. 000030774	0. 000043522
C3	O/P	0. 99554831	0. 033732950	0. 047703333
	O/F	1. 0000000	0. 000027181	0. 000038439
Components: 1-soil, 2-vegetation, 3-manmade. O/P-Original/Preliminary; O/P-Original/Final.				

(b) Four endmembers combination

Endmember		SCM	SAM	ED
C1	O/P	0. 75273329	0. 23198298	0. 32733832
	O/F	0. 99895786	0. 000000037	0. 000000021
C2	O/P	0. 99989903	0. 021801584	0. 030831495
	O/F	1. 0000000	0. 000000015	0. 000000035
C3	O/P	0. 99722484	0. 031696471	0. 044823703
	O/F	0. 99999998	0. 000039943	0. 000056586
C4	O/P	0. 99523259	0. 034829329	0. 049253619
	O/F	1. 0000000	0. 000027181	0. 000038439
Components: 1-water, 2-vegetation, 3-soil, 4-manmade. O/P-Original/Preliminary; O/P-Original/Final.				

Table 2. Spectral similarity measures between original and extracted spectra

4. VALIDATION OF HYPERION IMAGE

In this section the performance of the proposed algorithm was evaluated by applying on a Hyperion image. The hyperspectral image was captured by EO-1 Hyperion on Sep.7 2005 in Jiangyan area of Jiangsu Province and the image contained 167 bands after correction and processing (Datt, 2003) . For this experiment, a region covered a size of 60*60 pixels was chosen, after resampling the data bands, 50 contiguous bands (covering 508.22um to 1033.55nm) were selected from the dataset. Fig.11 (a) shows the study area in CIR, regions in red are covered with vegetation, of which the dark red are rice fields; roads and buildings are in cyan regions; and the region in black is water. Ground components in each area are relatively stable and fit for algorithm validation.

Three preliminary endmembers and endmembers extracted by the proposed algorithm were obtained. Compared with the spectra practically measured, the extracted three spectra are cotton, rice and water respectively. Applying LS and abundance fractions of extracted endmembers were estimated. Using these abundance fractions to rebuild the scene and then RMSE of the rebuilt scene were calculated to analyze the abundance estimated. The RMSE are 0.13349068, 0.13270831 by using the preliminary pure endmembers and the endmembers extracted by the proposed algorithm respectively, and the error decreased by applying the proposed algorithm.

Using the two kind endmembers to classify the scene by SAM method, classification results are shown in Fig.11, in (b) the regions marked A represent rice fields, the regions marked B are other vegetations and proved to be cotton fields; (c) is the classification result using SAM with preliminary pure pixels extracted by improved N-FINDR, (c) is the classification result using SAM with endmembers obtained by the researched method. Compared the three images, rice and cotton fields were well distinguished in (c), red regions represented rice fields and blue were rice fields respectively. However, in (d), the two crops were treated as one sort and the blue ones had no obvious meanings. SAM classification results also showed the advantage of this proposed algorithm.

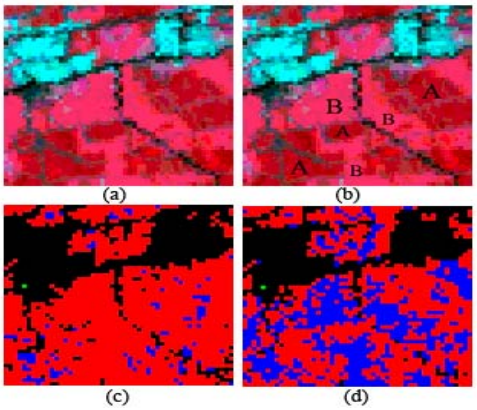

Figure 11. SAM classification results of Hyperion scene(a) Original scene in CIR; (b) Regions signed; (c) Classification with preliminary pure pixels; (d) Classification with the new endmembers

However, both RMSE calculated from the two scenes were comparatively higher due to that there were more than three

ground components in the scenes and the black areas in the classification images were ground covers didn't classified. Only extracted three endmembers and rebuilt the image could caused great errors, thus the algorithm that can extracted more endmembers is the next step to improve the classification precision. The result of SAM classification shows that the water hadn't be well extracted out, this may be caused for the pixels containing water also contained other ground covers thus affected the spectra of water. During the progress of the algorithm, it is found that in captured images, the spectral mixing of pixels is always performing as nonlinear and causes the deviations of extracted results. When extracting four endmembers in real images, there are some errors presented and how to judging the boundary pixels is quite significant. Further investigation is to overcome the limitation of linear mixing model. Although there are some shortages of linear mixing model, this algorithm still has higher extracting precision and has certain application value.

5. CONCLUSION AND DISCUSSION

(1) Aiming at the hyperspectral images which have no pure pixels and are formed by three or four ground components, a improved endmember extraction algorithm is proposed. The preliminary pure pixels formed the possible largest volume from the images are treated as mixing ones and through analysis it aims to extracted spectra which do not exit in the images as endmembers. Using the simulated images to validate the algorithm and the spectral similarity were measured, the advantage of this algorithm was proved. And the algorithm also applied on Hyperion image, comparing the SAM classification results and RMSE proved the advantage again.

(2) In real captured image, the effect of outside environment while obtaining the image and the performance of the sensor itself caused the nonlinear mixing of real ground components, convex polyhedron in N-D space is not as simple as assumed in linear mixing model but more complicated. When judging the boundary points, how to find the proper pixels is the most important step. Through setting the threshold, allowing the boundary points have small dissociation distances could solve the problem for certain degrees. However, this may cause the results relying on the threshold and boundary points would be very sensitive to the changing of threshold values. Thus how to choose the proper boundary points and overcome the problem under real complicated conditions are the stuffs need to be investigated next.

(3) The complexity of ground components also decides the abundance of information contained in image. Only suppose there are three or four endmembers to extract could not satisfy the application requirement, more endmembers extraction method should be put forward. Assuming images containing more than four endmembers, first to extract four endmembers, and then using orthogonal subspace projection to compress the fourth endmember information into the background formed by three preceding endmembers, and the fifth endmember could be extracted out in the tetrahedron in a compressed hyperplane. Repeat these steps until all the endmembers are extracted out.

REFERENCE

Agustin, Chang, J., 1999. Multispectral and Hyperspectral Image Analysis with Convex Cones. *IEEE Transactions on Geoscience and Remote Sensing*, USA, 37(2), pp. 756-770.

Antonio, J., 2002. Spatial/Spectral Endmember Extraction by Multidimensional Morphological Operations. *IEEE Transactions on Geosciences and Remote Sensing,* 40(9), pp. 2025-2041.

Antonio, J., 2004. A Quantitative and Comparative Analysis of Endmember Extraction Algorithms From Hyperspectral Data. *IEEE Transactions on Geoscience and Sensing*, USA, 42(3), pp. 650-663.

Bateson, J., 1993. A tool for manual endmember selection and spectral unmixing. *Summaries of the V JPL Airborne Earth Science Workshop*, Pasadena, CA.

Bateson, Asner, Wessman, J., 2000. Endmember bundles: A new approach to incorporating endmember variability into spectral mixture analysis. *IEEE Transactions on Geoscience and Remote Sensing*, USA, 28(3), pp. 1083–1094.

Bowles, J., 1995. Use of filter vectors in hyperspectral data analysis. Proc SPIE Infrared Spaceborne Remote Sensing III. Washington: SPLE Pub, pp. 148.

Chen, Tong, Guo, J., 1998. *Research on Mechanism of Remote Sensing Information.* Science Publishing Company, Beijing.

Datt, J. 2003. Preprocessing EO-1 Hyperion Hyperspectral Data to Support the Application of Agricultural Indexes. *IEEE Transactions on Geoscience and Remote Sensing*, USA, 41(6), pp. 1246-1259.

Geng. J., 2006. An automated endmember extraction algorithm based on volume of convex polyhedron in hyperspectral imagery. *Progress in natural science*, Beijing, 16(9), pp. 1196-1200.

Keshava, Mustard, J., 2002. Spectral unmixing. *IEEE Signal Processing Magazine*, USA, 19(1), pp. 44–57.

Kruse, J., 1998. Spectral identification of image endmembers determined from AVIRIS data. *Summaries of the VII JPL Airborne Earth Science Workshop.* Pasadena, CA.

Staenz, J., 1998. ISDAS - A system for processing /analyzing hyperspectral data. *Technical Note, Canadian Journal of Remote Sensin*g, CA, 24(2), pp. 99-113.

Theiler, J., 2000. Using blocks of skewers for faster computation of pixel purity index. *SPIE Int Conf Optical Science and Technology*, Washington: SPIE Pub, pp. 5-10.

Van der Meer. J, 2006. The effectiveness of spectral similarity measures for the analysis of hyperspectral imagery. *International Journal of Applied Earth Observation and Geoinformation 8*, Elsevier, Amsterdam, pp. 3-17.

Winter, J., 1999. N-FINDR: An Algorithm for Fast Autonomous Spectral Endmember Determination in Hyper Spectral Data. *Proc. SPIE Imaging Spectrometry,* Camarillo, CA, pp. 266-275.

Zhao, J., 2003. Theory and method of remote sensing application and analysis. Science Press, Beijing.

http://asterweb.jpl.nasa.gov/speclib/

ACKNOWLEDGEMENT

The authors extend their gratitude to the supports from: Jiangsu province high-tech project (BG2006340), Project of Commission of Science Technology and Industry for National Defence (2006A02A100602), National scientific and technological support project (2006BAK30B01).